



Coalescing drops in microfluidic parking networks: A multifunctional platform for drop-based microfluidics

Swastika S. Bithi, William S. Wang, Meng Sun, Jerzy Blawdziewicz, and Siva A. Vanapalli

Citation: *Biomicrofluidics* **8**, 034118 (2014); doi: 10.1063/1.4885079

View online: <http://dx.doi.org/10.1063/1.4885079>

View Table of Contents: <http://scitation.aip.org/content/aip/journal/bmf/8/3?ver=pdfcov>

Published by the [AIP Publishing](#)

Articles you may be interested in

[Coplanar electrowetting-induced stirring as a tool to manipulate biological samples in lubricated digital microfluidics. Impact of ambient phase on drop internal flow pattern](#)

Biomicrofluidics **7**, 044104 (2013); 10.1063/1.4817006

[Geometrical effects in microfluidic-based microarrays for rapid, efficient single-cell capture of mammalian stem cells and plant cells](#)

Biomicrofluidics **6**, 024112 (2012); 10.1063/1.4704521

[An integrated, multiparametric flow cytometry chip using “microfluidic drifting” based three-dimensional hydrodynamic focusing](#)

Biomicrofluidics **6**, 024113 (2012); 10.1063/1.3701566

[Hydrogel discs for digital microfluidics](#)

Biomicrofluidics **6**, 014112 (2012); 10.1063/1.3687381

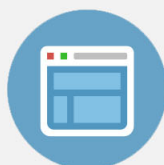
[A robotics platform for automated batch fabrication of high density, microfluidics-based DNA microarrays, with applications to single cell, multiplex assays of secreted proteins](#)

Rev. Sci. Instrum. **82**, 094301 (2011); 10.1063/1.3636077

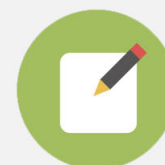


Re-register for Table of Content Alerts

Create a profile.



Sign up today!



Coalescing drops in microfluidic parking networks: A multifunctional platform for drop-based microfluidics

Swastika S. Bithi,¹ William S. Wang,¹ Meng Sun,¹ Jerzy Blawdziewicz,²
and Siva A. Vanapalli^{1,a)}

¹*Department of Chemical Engineering, Texas Tech University, Lubbock, Texas 79409–3121, USA*

²*Department of Mechanical Engineering, Texas Tech University, Lubbock, Texas 79401–1021, USA*

(Received 4 April 2014; accepted 13 June 2014; published online 25 June 2014)

Multiwell plate and pipette systems have revolutionized modern biological analysis; however, they have disadvantages because testing in the submicroliter range is challenging, and increasing the number of samples is expensive. We propose a new microfluidic methodology that delivers the functionality of multiwell plates and pipettes at the nanoliter scale by utilizing drop coalescence and confinement-guided breakup in microfluidic parking networks (MPNs). Highly monodisperse arrays of drops obtained using a hydrodynamic self-rectification process are parked at prescribed locations in the device, and our method allows subsequent drop manipulations such as fine-gradation dilutions, reactant addition, and fluid replacement while retaining microparticles contained in the sample. Our devices operate in a quasistatic regime where drop shapes are determined primarily by the channel geometry. Thus, the behavior of parked drops is insensitive to flow conditions. This insensitivity enables highly parallelized manipulation of drop arrays of different composition, without a need for fine-tuning the flow conditions and other system parameters. We also find that drop coalescence can be switched off above a critical capillary number, enabling individual addressability of drops in complex MPNs. The platform demonstrated here is a promising candidate for conducting multistep biological assays in a highly multiplexed manner, using thousands of submicroliter samples. © 2014 AIP Publishing LLC.

[<http://dx.doi.org/10.1063/1.4885079>]

I. INTRODUCTION

Biological and biomedical applications such as drug screening,^{1,2} cellular assays,^{3,4} DNA analysis,^{5,6} and protein crystallization^{7,8} require high-throughput manipulation of multiple fluid samples of precisely specified volumes and composition. Complex multistep assays rely upon dispensing well-controlled amounts of reagents into each sample at specified times as well as sample dilution and removal of excess fluid. Moreover, suspended solid particles (such as cells) are often the key component of the system and need to be retained when samples are manipulated.

Multiwell plates and automated pipetting systems have revolutionized modern biological analysis, providing the above functionality. The multiwell storage allows easy barcoding for identification and retrieval of samples, and pipettes can dispense known volumes of fluids into wells. However, these systems suffer from a critical constraint: it is difficult to scale down sample size to submicroliter volume, due to fluid evaporation and pipetting errors.^{9,10} Since small volumes are crucial to large-scale high-throughput devices in which numerous samples are manipulated simultaneously, throughput of current multiwell-plate/pipette systems is limited.

^{a)}Author to whom correspondence should be addressed. Electronic mail: siva.vanapalli@ttu.edu

Moreover, sample/reagent volumes ultimately determine the diversity of biological assays that can be conducted.

Drop-based microfluidics has the potential to bring about a paradigm shift in fluid handling and manipulation at the submicroliter scale.^{11–14} Rapid production of monodisperse drops^{15,16} has already enabled large-scale assays in which millions of picoliter-volume drops served as individual reaction chambers.^{17–20} However, this exquisite ability to downscale fluid volumes using microfluidic drops is not yet accompanied by techniques for manipulating individual drop volumes with the same easiness and flexibility as multiwell-plate/pipette systems. For example, current drop-storing methods^{21–28} are not flexible enough to yield drops of controllable volume as they require simultaneous optimization of drop size, flow conditions, and network architecture. Moreover, very little progress has been made on modifying the contents of stored drops.²⁹

Recent development of microfluidic parking networks (MPNs) to generate and manipulate static drop arrays (SDAs)^{22,24,30} has been an important step towards achieving in microfluidic devices the functionality of automated multiwell-plate/pipette systems. As shown in Fig. 1(a), an MPN consists of a series of interconnected parking loops; each loop has a bypass channel and a lower branch containing a fluidic trap. When a train of drops passes through an MPN, the drops are sequentially parked in the traps (Fig. 1(a)), and the rest of the drop train travels through bypass channels. Similar to individual wells in multiwell plates, the parked drops have well-defined geometrical positions, which enable easy sample identification.

However, the use of non-coalescing drops by adding excess surfactant (a standard practice in the drop-based microfluidics) in current parking networks hinders their potential to serve in

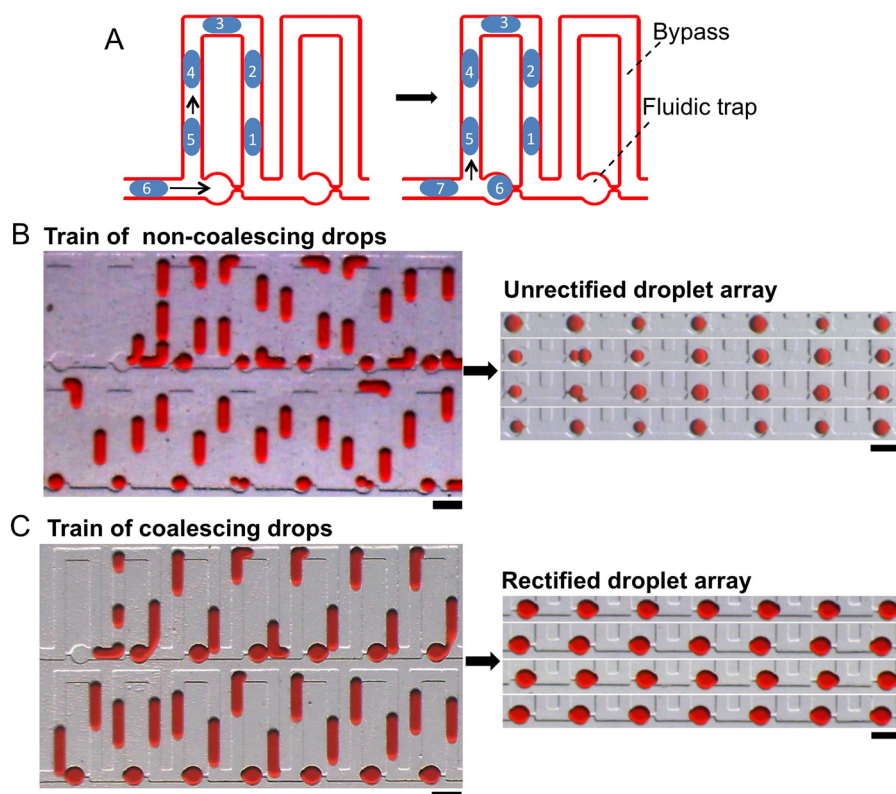


FIG. 1. Droplet storage using a train of small drops. (a) An MPN with each parking loop containing a bypass channel and a fluidic trap. Due to a difference in the resistance ratio of the branches, a drop is parked in the trap. The droplet train is produced by an upstream T-junction. (b) Injection of a train of non-coalescing drops into the MPN produces polydisperse static droplet arrays. 2 wt. % Span 80 in. mineral oil was used as continuous phase to prevent coalescence. (c) Highly monodisperse arrays are generated when a train of coalescing drops is injected into the MPN. Mineral oil with no added surfactant was used as the continuous phase to induce drop coalescence. Scale bar is 500 μm . (Multimedia view) [URL: <http://dx.doi.org/10.1063/1.4885079.1>] [URL: <http://dx.doi.org/10.1063/1.4885079.2>]

the integrated devices for biological analysis. The key obstacles (described in more detail in Sec. II A) include (i) difficulties in obtaining highly monodisperse drop arrays due to natural instabilities of the flow in the parking network (see Fig. 1(b) (see integral multimedia file Fig. 1(b))); (ii) problems with handling suspended particles (such as cells); and (iii) lack of methods for controlled reagent addition and removal (only recently have attempts been made in this direction²⁹).

We show that all three issues can be solved by replacing non-coalescing drops with coalescing drops in which the surfactant concentration is tuned, and harnessing coalescence between moving drops and trapped drops, followed by a confinement-guided breakup. The volume of a trapped drop after breakup is determined primarily by the geometry of the trap and bypass channel and is insensitive to flow conditions (provided that the capillary number is small). Thus, when a train of drops passes through an MPN, a series of coalescence and breakup events produces an SDA with highly controllable reproducible volumes. We refer to this novel collective flow regime, illustrated in Fig. 1(c) (see integral multimedia file Fig. 1(c)), as hydrodynamic self-rectification.

A similar coalescence and breakup process allows for reagent addition and removal. As demonstrated in our study, the addition and removal operations can be performed while retaining solid particles enclosed in the trapped drops. In what follows, we show that the processes of hydrodynamic self-rectification and fluid exchange are sufficiently robust to be used in complex multiplexed networks, without a need for precise optimization of system geometry and flow parameters. Thus, MPNs with coalescing drops not only provide the essential functionality of multiwell-plate/pipette system, but are also a promising candidate for developing large-scale multiplexed devices for high-throughput assays.

II. RESULTS AND DISCUSSION

A. Limitations of current approaches to store drops in MPNs

1. A train of small drops

In a typical MPN experiment, a train of non-coalescing surfactant-covered drops of volume V_d comparable to the trap volume V_T is injected into the device, since drops smaller than the trap cannot be effectively stored due to lower squeeze-through threshold.^{22,30} Leading drops of the train enter the bypass channel, thus increasing its resistance. When the resistance exceeds a threshold value (determined by the trap-channel geometry), the next drop enters the trap where it gets parked (Fig. 2(a) (see integral multimedia file Fig. 2(a))). This process repeatedly occurs at subsequent traps.

This simple method is capable of producing SDAs for a relatively wide range of conditions. However, as shown in Fig. 2(b), *monodisperse* arrays with drops of well-controlled volumes are obtained only in a narrow region of the control-parameter space. This restriction severely limits the flexibility of the approach and its usability in large-scale applications.

Key hydrodynamic mechanisms that cause nonuniform size distribution of parked drops are illustrated in Fig. 2. These mechanisms include (i) development of highly nonuniform drop spacing due to the hydrodynamic coupling through the connected trap and bypass channels (cf. Fig. 2(a)); and (ii) drop breakup at the trap entrances, induced by encounters of two closely spaced drops (cf. Fig. 2(c)). The above mechanisms are interrelated: the irregular drop spacing in the MPN produces varying conditions at the trap inlets causing frequent collision-induced breakup events and, therefore, polydispersity of arrays in majority of the tested flow conditions.

The highly nonuniform drop spacing is an intrinsic feature associated with the network topology. As illustrated in Fig. 2(d), when a drop enters the bypass channel, more fluid leaks through the trap channel allowing the trailing drops to catch up. After a drop is parked in the trap, the leak stops, and therefore, the drop spacing does not recover at the exit of the bypass channel. Simplified numerical simulations where drops are treated as mobile point-like fluidic resistors³¹ reveal that the distance between drops keeps decreasing as more loops are traversed (Fig. 2(e), see integral multimedia file Fig. 2(e) (upper)). This natural hydrodynamic instability

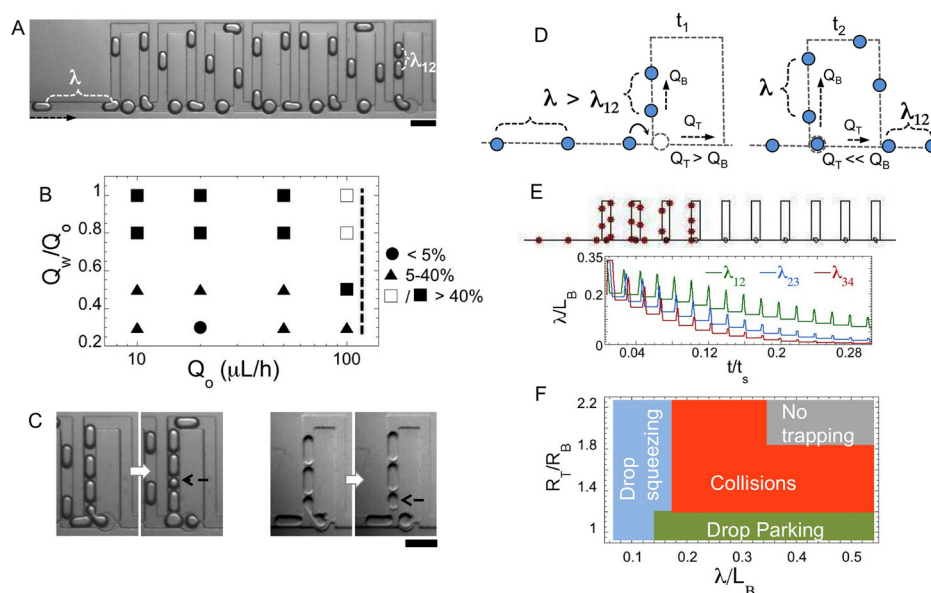


FIG. 2. Hydrodynamic mechanisms responsible for polydispersity in arrays of non-coalescing drops. (a) A train of drops in the MPN. The distance λ_{12} between the leading drops is significantly reduced compared to the spacing λ at the network entrance. The arrow indicates flow direction. (b) Polydispersity of SDAs obtained in the device shown in panel “a” for different water and oil flow rates Q_w and Q_o . For the flow conditions reported, the drop volume normalized with trap volume is $V_d/V_T = 0.6 - 1.7$, and the drop spacing normalized with bypass length is $\lambda/L_B = 0.2 - 0.5$. Only a single point corresponds to polydispersity smaller than 5%. For polydispersity above 5%, the open and closed symbols indicate droplet dynamics dominated by collision-induced and flow-induced drop breakup events, respectively. The dashed vertical line marks the flow rate above which drops squeeze through the trap channel. (c) Collision-induced (left) and elongational-flow-induced (right) breakup of drops. Black arrows indicate drop fragments. (d) Reduction of drop spacing at the head of the train is caused by fluid leak through the trap channel. Initially the flow rate through the trap channel Q_T is comparable to the flow rate through the bypass channel Q_B . After a drop is parked, the trap channel is blocked, $Q_T \ll Q_B$, and thus the drop spacing in the train head does not return to its initial value at the exit of the bypass channel. (e) (Upper) Simulation of droplet traffic in the microfluidic parking network showing crowding of drops in the bypass. The simulation parameters are: $R_B = 2.13 \text{ kg/s}\cdot\text{mm}^4$, $R_T = 4 \text{ kg/s}\cdot\text{mm}^4$, $Q = 180 \text{ }\mu\text{L/h}$, $\beta = 1.2$, $R_d = 0.5 \text{ kg/s}\cdot\text{mm}^4$, $R_{id} = 3 \text{ kg/s}\cdot\text{mm}^4$, $\lambda = 1333 \text{ }\mu\text{m}$ and $\Delta P_L = 300 \text{ Pa}$, number of traps = 10, and number of drops = 30. (Lower) A representative drop traffic simulation showing that the relative distance between drops at the head of the train decreases with time, consistent with the experimental observation in Fig. 2(a). The drop spacing λ is normalized by the bypass length L_B and the time t by the total simulation time t_s . (f) State diagram generated by the traffic simulations with different trap-to-bypass resistance ratios R_T/R_B and droplet spacing λ . The regime of drop parking is very narrow. Details of the simulations are described in supplementary material.³⁶ In Figs. (a)–(c), 2 wt. % Span 80 in. mineral oil was used to produce non-coalescing drops. (Multimedia view) [URL: <http://dx.doi.org/10.1063/1.4885079.3>] [URL: <http://dx.doi.org/10.1063/1.4885079.4>]

persists over a wide range of inlet drop-spacing values and branch-resistance ratios (Fig. 2(f)), resulting in collisions and the associated drop polydispersity.

2. Parked drops produced by a long plug

The above instability can be avoided by replacing a train of short drops with a single long plug of volume much greater than the trap volume, $V_d/V_T \gg 1$.^{24,29} As shown in Fig. 3, after a portion of the plug fills a trap, the tail of the plug arrives at the junction and breaks off, leaving a parked drop with a well-defined size determined by the trap volume.

This method produces highly monodisperse SDAs and works well with soluble reagents (Fig. 3(a)). However, it is not suitable for storing drops that contain insoluble materials such as cells or microparticles, because particles segregate to the rear of the plug producing parked drops with composition that varies in an uncontrollable manner (Fig. 3(b)). The non-uniform material distribution is caused by particle sedimentation across micron-scale channel depths, resulting in slower particle movement compared to the average fluid velocity.^{32,33} The long-plug method also has other problems, such as the need for optimization of the number and volume of long plugs as the size of the MPN increases.

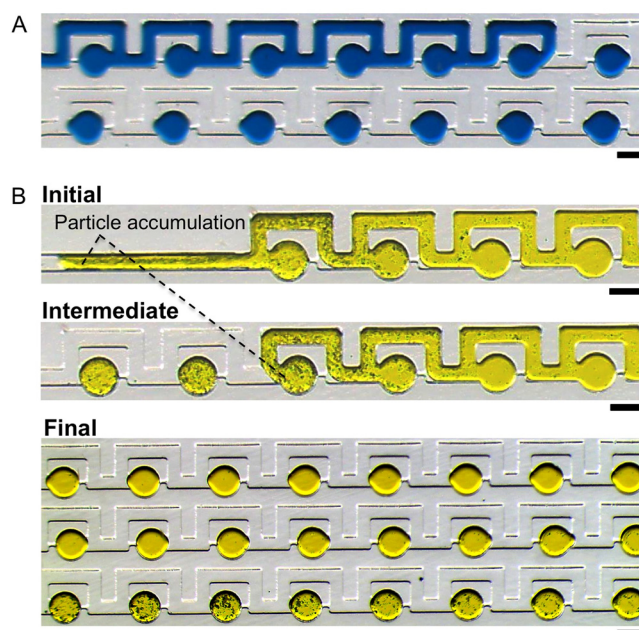


FIG. 3. Storage of drops using long plugs. (a) A plug of soluble reagent is fragmented at junctions leaving a monodisperse droplet array. (b) Insoluble particles (polystyrene beads of diameter $10\ \mu\text{m}$) segregate to the rear of the long plug due to gravitational effects, resulting in a droplet array with nonuniform distribution of particles. 2 wt. % Span 80 in. mineral oil was used as continuous phase. Scale bar is $500\ \mu\text{m}$.

B. Hydrodynamic self-rectification

As shown above, current methods for generating SDAs using a train of non-coalescing drops suffer from flow instabilities that lead to polydispersity of the array of parked drops. This poor control of drop volume hampers broader applications of MPN-based techniques. Here, we demonstrate that switching from non-coalescing to coalescing drops by tuning surfactant concentration eliminates the polydispersity problem. Because drops are capable of coalescence, polydispersity is eliminated by correcting volumes of parked drops after the SDA has been created. The volume correction, achieved via the hydrodynamic self-rectification process provides a robust and flexible method for creating and manipulating SDAs.

1. Basic mechanism

As illustrated in Figs. 1(c) and 4(a), the hydrodynamic self-rectification involves momentary coalescence between drops of a moving train and a drop parked in an underfilled or overfilled trap. Drop coalescence at the trap entrance is followed by detachment of a drop carrying away the excess fluid. This process produces a parked drop with corrected volume determined by the trap geometry. The detachment of the moving drop occurs under quasistatic conditions,³⁴ because the flow-based capillary number is small, $Ca = \mu_o U / \gamma \ll 1$ (where μ_o is the viscosity of the carrier phase, U is the total mean fluid velocity, and γ is the interfacial tension). The shape of the interface during the breakup event is thus insensitive to the flow conditions, and therefore, the drop volume is primarily determined by the geometry of the trap and the junction between the trap and bypass channels (Fig. 4(b)).

Our experiments show that as the self-rectification process progresses, the monodispersity of the array further improves. This is because when all traps are already filled, there is little flow through the trap channels, and therefore the drops in the trailing part of the moving train maintain uniform spacing. Thus, trailing and parked drops experience nearly identical rectification conditions at every loop, resulting in highly monodisperse SDAs.

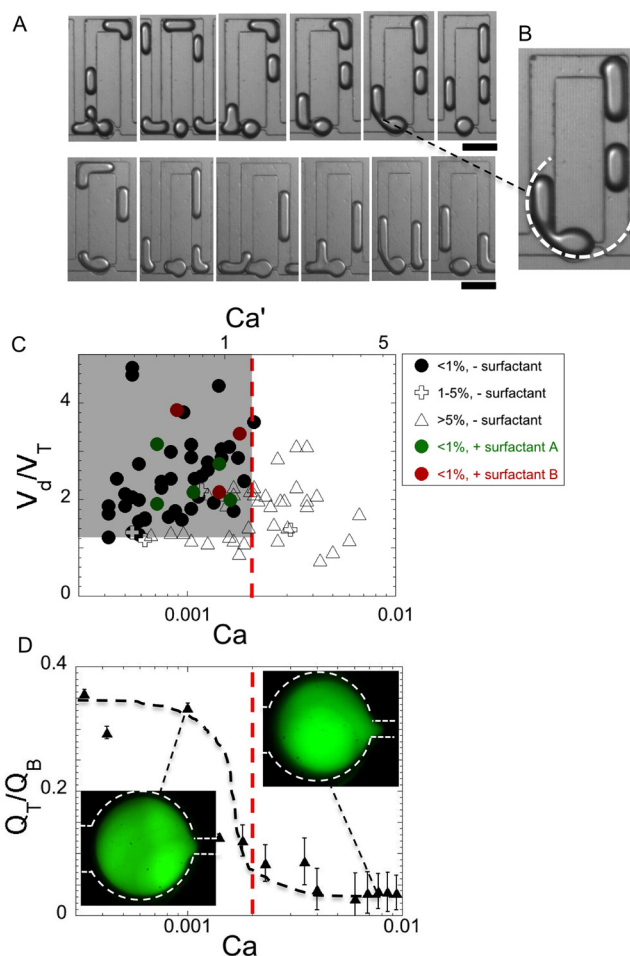


FIG. 4. Mechanism of hydrodynamic self-rectification. (a) Rectification of drop volume when trap is underfilled (upper) and overfilled (lower). (b) Geometry-guided breakup of a confined drop at the junction. Quasi-static shape of the drop is circular (indicated by white arc) because of pressure drop across the interface. (c) The polydispersity map for coalescing drops. The drop-to-trap volume ratio V_d/V_T and capillary number Ca determine the regime of self-rectification. The parameter space where monodisperse arrays are obtained is wide (indicated by the gray shaded area). The top axis represents the rescaled capillary number Ca' based on the pressure drop across the trap. The rectification boundary (dashed vertical line) occurs at $Ca' = O(1)$. The black, green and red symbols represent experiments where the continuous phase is mineral oil with no added surfactant, 0.001 wt. % fluorosurfactant (KrytoxFSH-PEG600-KrytoxFSH) in FC-40 and 10 vol. % alcohol-based surfactant (1H, 1H, 2H, 2H-perfluoro-1-octanol) in FC-40, respectively. (d) The measured carrier-fluid flow-rate ratio Q_T/Q_B between the trap and bypass channels as a function of capillary number in the presence of a parked drop. Rectification does not occur above a critical capillary number (dashed vertical line), when the flow rate dramatically decreases in the trap. The error bar represents the standard deviation of the centerline particle velocity measurements in the bypass. The insets show images of parked drops in the trap at low and high capillary numbers. At the higher capillary number the parked drop deforms and blocks the constriction at the trap outlet. Scale bar is $500 \mu\text{m}$.

2. Regime of self-rectification

To identify the limits of operability of the rectification mechanism, we conducted a series of experiments in which the size, spacing, and mean velocity of the drops in the train entering the MPN were varied (which was achieved with the help of auxiliary side-channels downstream of the drop generator). Fig. 4(c) with two independent parameters, the drop-to-trap volume ratio V_d/V_T and capillary number Ca , shows the rectification region in which monodisperse SDAs were obtained. The rectification domain $V_d/V_T > 1$ and $Ca < Ca^* = 0.002$ is large, demonstrating that the method for drop-volume correction is highly flexible, and no precise optimization of system parameters is needed. Moreover, since highly monodisperse arrays can also be achieved with surfactant-covered drops (see Fig. 4(c)), the rectification method can be used in

biological assays where biocompatible surfactants are needed to prevent adsorption and transport of biomolecules across the drop interface.

The self-rectification phenomenon was not observed above the critical capillary number Ca^* . Our analysis shows that for $Ca > Ca^*$, the parked drop deforms significantly, blocking the constriction in the trap. As a result, fluid flow through the trap channel is reduced, and passing drops do not penetrate into it deeply enough for coalescence with the parked drop to occur. Consistent with this mechanism, the border of the self-rectification region represented in terms of the rescaled capillary number $Ca' = \Delta P w / \gamma$ (where ΔP is the pressure drop across the trap and w is the trap diameter) is $Ca' = O(1)$, as indicated by the top scale in Fig. 4(c). This physical picture is further confirmed by images of the drop shape in the trap and by the measurements of the flow-rate ratio Q_T/Q_B between the trap and bypass channel, depicted in Fig. 4(d).

In the above analysis, ΔP is assumed to be as the pressure gradient when the parked drop fully blocks the constriction, which is given by $\Delta P \approx Q_M R_B$, where Q_M and R_B are the total flow rate and hydrodynamic resistance of the bypass channel. The hydrodynamic resistance of the bypass is calculated from the length, width, and height of the bypass channel using the analytical equation for hydrodynamic resistance of a rectangular channel.³⁵ These two quantities are known from the bypass geometry and the total flow rate supplied to the device allowing us to determine ΔP and the rescaled capillary number.

C. Fluid manipulation in arrays of stored drops

1. Precisely controlled exchange of fluids

The mechanism responsible for hydrodynamic self-rectification (i.e., drop coalescence followed by the geometry-guided breakup) also provides simple means for controlled fluid exchange between the parked and moving drops. Such a two-way fluid transfer is illustrated in Fig. 5(a) (see integral multimedia file Fig. 5(a)), which presents a series of encounters between a stationary drop preloaded with reagent and water drops in a train moving through the bypass channel.

The images show a steady decrease of the reagent concentration in the parked drop, C_p . The concentration evolution is quantitatively represented in Fig. 5(b) for two sizes of passing drops. Since a fixed fraction α of the stationary-drop fluid is replaced at each encounter, the reagent concentration C_p decreases by the factor $1 - \alpha$ as a result of a coalescence/breakup event. It follows that the reagent concentration evolves according to the geometric progression:

$$C_P = (1 - \alpha)^N C_0, \quad (1)$$

where N is the number of encounters, and C_0 is the initial reagent concentration.

The experimental results presented in Fig. 5(b) agree well with Eq. (1), showing a fine gradation of dilution with α of the order of several percent. This dilution step size is far smaller than the one obtained using pipettes and can be controlled by the drop-size ratio and channel geometry.

The rectification-inspired fluid-exchange method can be used to add or remove reagents from stored drops at well-defined time points, similar to the functionality of pipettes. Moreover, analogous to serial dilutions created by pipettes, the basic concept of dilution can be expanded to precisely control fluid exchange between several stored drops, producing static drop arrays with fine gradation in composition (Fig. 5(c) (see integral multimedia file Fig. 5(c)), see also Ref. 29). The concentration gradation and range in the array can be simply manipulated by volumes and initial composition of moving and stored drops.

2. Reagent removal from particle-loaded droplet arrays

The gravitational settling of particles that hampers applicability of long plugs for storage of insoluble materials (see Fig. 3(b)) can be exploited in the small drops to retain particles at the bottom of the drop, while fluid-exchange is performed by moving coalescing drops. This

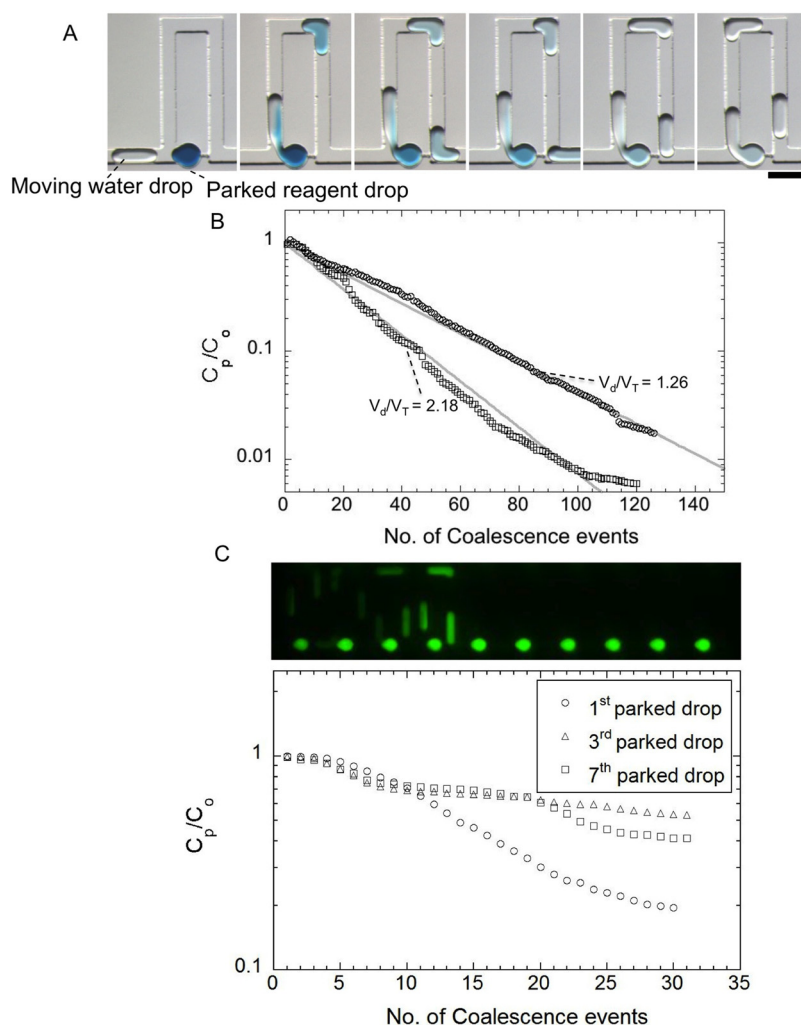


FIG. 5. A simple drop-dilution system inspired by hydrodynamic self-rectification. (a) Coalescence-induced transfer of reagent (blue dye) from a parked drop to moving water drops. The dilution process is shown over 10 min (120 coalescence events). Reagent concentration gradually decreases, resulting in a drop train that has fine concentration gradation. The continuous phase is mineral oil with no added surfactant. (b) Normalized reagent concentration in the parked drop C_p/C_o as a function of number of the coalescence events for two different volumes of moving water drops normalized by the trap volume V_d/V_T . Symbols are experimental data, and solid lines represent dilution model (1) with $\alpha = 0.0315$ and 0.0475 , respectively. (c) (Top) Drop dilution using multiple microfluidic parking loops (10 loops). Reagent (fluorescent dye) concentration variation is observed in both the stationary and moving drops. (Bottom) The corresponding normalized reagent concentration in the parked drops as a function of the number of coalescence events for several trapped drops having same volume but different locations in the MPN. As expected we find that the reduction in reagent concentration is much more for the first parked drop than the parked drops located further downstream in the MPN. The 3rd drop concentration is higher than the 7th drop due to some moving drops not coalescing with the 3rd parked drop. The MPN geometry is same as that of Fig. 1. Scale bar is $500\ \mu\text{m}$. (Multimedia view) [URL: <http://dx.doi.org/10.1063/1.4885079.5>] [URL: <http://dx.doi.org/10.1063/1.4885079.6>]

approach is very similar to exchanging fluids in multiwells after cells have sedimented. Fig. 6 demonstrates this ability to replace fluids while particles are retained in drops.

As shown in Fig. 6(a), coalescing drops containing particles can be injected into the MPN, and monodisperse particle-laden droplet arrays can be produced using the rectification method (Fig. 6(b)). The particle distribution in the rectified static drops closely follows Poisson statistics (see Fig. 6(c)). The dye in the particle-loaded drops is replaced by coalescing water drops (Fig. 6(d) (see integral multimedia file Fig. 6(d))), mimicking the washing steps performed with pipettes in multiwell plates. Figure 6(e) shows the final outcome, where the original fluid from all the drops is removed without significant change in the number of particles (Figs. 6(f) and 6(g)).

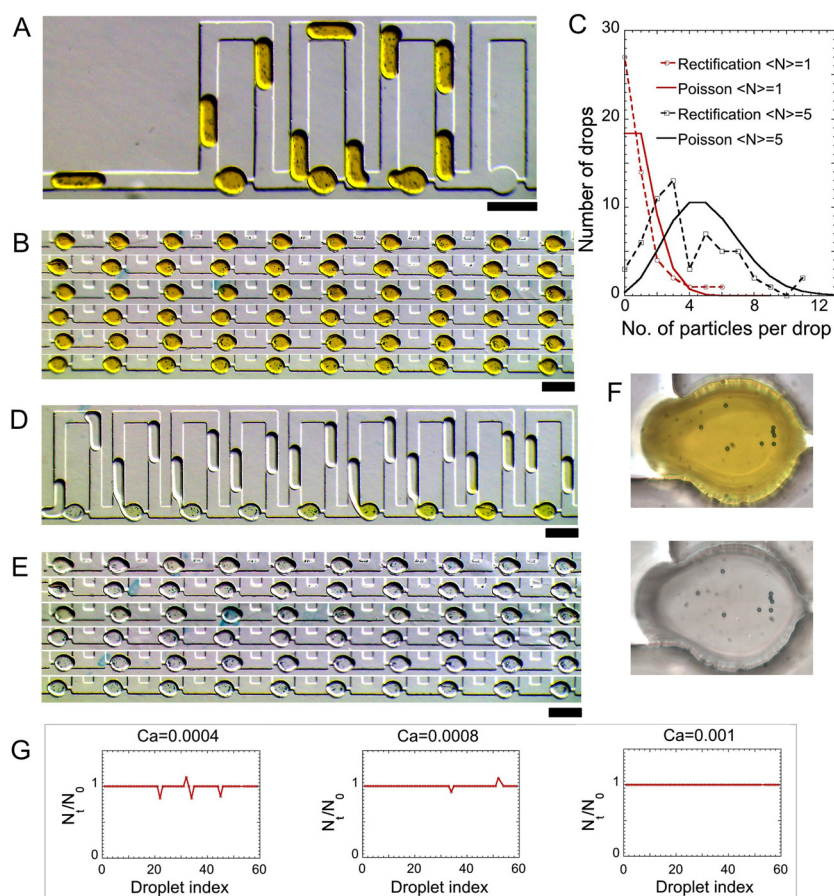


FIG. 6. Reagent manipulation in particle-loaded drop arrays. (a) Parking and self-rectification of coalescing drops containing a mixture of particles (polystyrene beads of diameter $10\ \mu\text{m}$) and a reagent (yellow dye). (b) Monodisperse droplet array with a reagent and Poisson-like particle distribution. (c) The measured distribution of particles in the drop array compares well with the Poisson distribution. Results are shown for two systems with different mean number of particles per drop (N). (d) The reagent is washed away from the particle-laden static drops by injection of a new water plug. (e) Image showing that the reagent is washed away while particles are retained. (f) Higher resolution image of a representative drop before and after washing. (g) Plots show the ratio N_t/N_0 of the number of particles retained in each drop in the array to those present prior to washing. The data is shown for washing step conducted at three different capillary numbers. The continuous phase is mineral oil with no added surfactant. Scale bar is $500\ \mu\text{m}$. (Multimedia view) [URL: <http://dx.doi.org/10.1063/1.4885079.7>]

This ability to retain particles while soluble reagents are being added or removed persists over a sufficiently broad range of capillary numbers (see Fig. 6(g)).

D. Versatility of coalescence-based approach

The results presented in Secs. II B and II C show that MPNs with coalescing drops can provide the essential functionality of multiwell-plate/pipette systems. In particular, highly monodisperse submicroliter size SDAs can be created using hydrodynamic self rectification mechanism, reagents can be added to or removed from the static drops on demand, and the technique is well suited for manipulating fluids with suspended particles.

We have also shown that the parameter space where geometry-controlled momentary coalescence of drops occurs is large, and due to the geometry-guided breakup mechanism the resulting sizes of parked drops are insensitive to flow conditions (such as the flow rate and size of moving drops in delivery trains). Our MPN-based techniques can thus be used without elaborate optimization of the system parameters. This robustness of the method makes it well suited for engineering large-scale systems of coupled MPNs.

The versatility and flexibility of the coalescence-based MPN techniques is illustrated in Fig. 7. We can produce highly monodisperse static arrays of hundreds of drops (Fig. 7(a) shows an array of 384 drops, which is a typical number of wells in a multiwell plate). Furthermore, not only monodisperse SDAs can be obtained but also arrays with varying drop volumes predetermined by the size of microfluidic traps (Fig. 7(b) presents an SDA with drop volumes gradually decreasing from 25 nL to 5 nL). Our method is also suitable for multiplexing using coupled MPNs controlled by shared fluid sources to reduce operational complexity of parallelization. Fig. 7(c) shows a network with four hydrodynamically coupled drop generators to deliver fluids of different composition using a single source of the carrier fluid. Fig. 7(d) presents an alternative MPN design consisting of 24 inlet reservoirs, each loaded with a different reagent delivered using a common suction pressure at the outlet. All the above tasks can be achieved using nanoliter to microliter size drops (i.e., volumes several orders of magnitude smaller than the minimal volume in multiwell plates).

Our methods offer a promising substitute for multiwell plates and robot-aided pipettes, with benefits of substantially smaller sample volumes and reagent consumption, highly parallelized analysis, and competitive throughput. We estimate that $O(10^4)$ drops can be parked in a footprint equivalent to a conventional multiwell plate (see supplementary material text 1.1³⁶). Given that drop parking and rectification rate ranges from 1 to 10 drops per second (which is typical of geometry-driven breakup processes¹⁶), we can perform parallelized storage in several minutes. A similar timescale will be needed to perform tasks such as reactant addition or removal.

III. CONCLUSIONS AND OUTLOOK

Drop-based microfluidics is one of the most promising technologies for lab-on-chip applications, where submicroliter-size drops serve as natural miniaturized reaction chambers. The

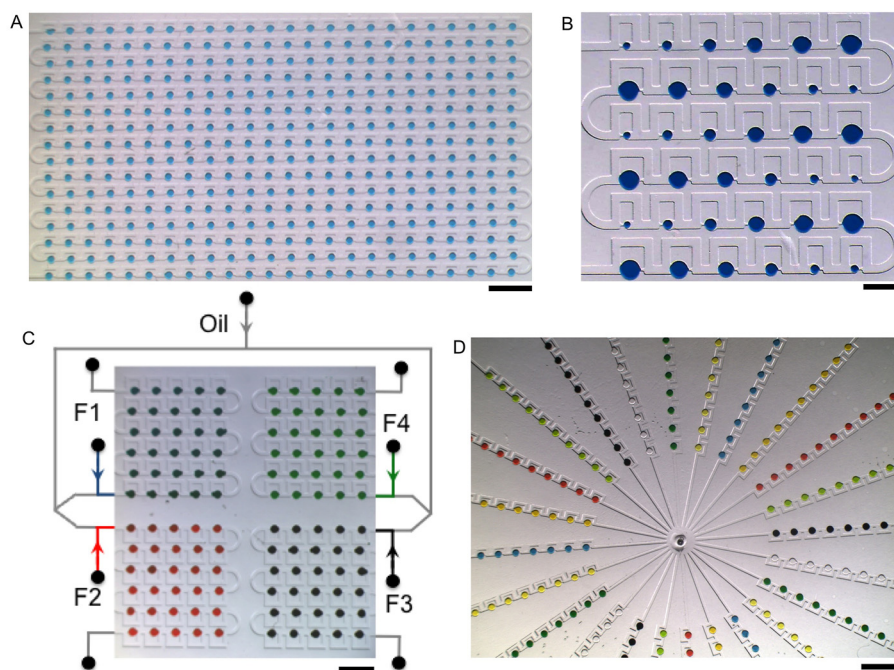


FIG. 7. Versatile functionality delivered by coalescing drops in MPNs. (a) An array of 384 uniform-sized drops of volume 2 nL. (b) A droplet array with rows of gradually varying fluid volumes ranging from 5 to 25 nL. (c) Multiplexed static drop arrays produced using a parallelized network containing four hydrodynamically coupled drop generators F1–F4 and sharing the same oil source. (d) Simultaneous storage of 24 SDAs of different composition. A microliter of each fluid is loaded at the inlet reservoir and aspirated using a common suction pressure at the outlet. The continuous phase is mineral oil with no added surfactant. Scale bar is 2 mm.

small volumes and easiness with which numerous drops can be generated make drop-based microfluidics a natural candidate for developing high throughput systems for biological-analysis applications.

While some large-scale applications have been demonstrated,^{17,18} they are mostly limited to processes where identical initial conditions in each drop are sufficient, and no manipulation of drop content is necessary after creating the initial state. The techniques developed here overcome these limitations, and therefore may bring a paradigm shift in drop-based microfluidic applications. We have shown that storing drops in prescribed places and precise manipulation of drop content can be achieved in a simple and versatile system with an inexpensive world-to-chip interface (in contrast to much more complex valve-based microfluidic technology³⁷).

The capabilities demonstrated herein can be used in a variety of configurations, ranging from simple inexpensive assays with drops manipulated by a hand-operated syringe to complex multiplexed systems with thousands of drops whose content is controlled in space and time using a small number of pressure sources. With a proper time control of the flow rates through the parking network, the proposed methodology may allow not only global fluid exchange in entire static arrays, but also ensure individual drop addressability (since the coalescence between the parked and moving drops is switched off above the critical capillary number). In situations where passive coalescence may not be achievable, for example, due to excess surfactant, electrocoalescence^{38,39} can be used to trigger on-demand fluid addition or replacement providing sophisticated functionalities for drop-based microfluidics.

The proposed drop-based MPN platform complements existing high throughput droplet devices by providing the multiwell plate functionality (which is currently lacking). The platform has significant potential for multi-step biological analysis where reagents need to be added to or removed from stored drops, for example, in cell culture and cytotoxicity assays. Our techniques may therefore help to transform drop-based microfluidics into a powerful and versatile technology for precise fluid manipulation at the submicroliter scale.

IV. MATERIALS AND METHODS

A. Device design and fabrication

We fabricated polydimethyl siloxane (PDMS) devices using soft lithography.⁴⁰ For details of the device design and dimensions of the branches and traps, see supplementary material Tables S1 and S2.³⁶

B. Materials

The dispersed phase is either water or aqueous solutions of food dyes. The continuous phase used in the experiments and the corresponding interfacial tension values are (i) embryonic mineral oil (Sigma Aldrich, Part M5904, $\mu_o = 30 \text{ mPa}\cdot\text{s}$) with no added surfactant, $\gamma = 50 \text{ mN/m}$ (measured using Kruss K100 tensiometer, Kruss, NC) (ii) embryonic mineral oil with 2 wt. % Span 80 (Sigma Aldrich), $\gamma = 5 \text{ mN/m}$ ⁴¹ (iii) FC-40 (Acros Organics, Part AC12376-1000, $\mu_o = 4.1 \text{ mPa}\cdot\text{s}$) containing 0.001 wt. % biocompatible fluorosurfactant, KrytoxFSH-PEG600-KrytoxFSH (RAN Biotechnologies, Inc., MA), $\gamma = 40 \text{ mN/m}$ (Ref. 42) (iv) FC-40 containing 10 vol. % 1H, 1H, 2H, 2H-perfluoro-1-octanol (Acros Organics), $\gamma = 16 \text{ mN/m}$ (measured using Kruss K100 tensiometer, Kruss, NC). The figure captions list which continuous phase was used for the corresponding experiments. For Figs. 3(b) and 6, black dyed polystyrene beads (10 μm diameter, Polysciences) at particle densities of 5×10^5 per mL were used.

C. Microfluidic experiments

Trains of small confined drops are injected into the MPN by controlling the aqueous and oil flow rates Q_w and Q_o at an upstream T-junction, using syringe pumps (PHD2000, Harvard Apparatus). Long plugs were generated using a cartridge method.⁸ Experiments were conducted on a stereo microscope (SZX16, Olympus) and inverted microscopes (IX-70 and IX-71, Olympus). Movies were recorded using high-speed cameras (PCO1200, Cooke Corp; Phantom

v310, Vision Research Inc. and StreamView-LR, SVSI) and still images were acquired using a color camera (PL-B776F, PixeLINK; Edmund Optics). Images were analyzed to determine the polydispersity in the droplet array. Both the capillary number $Ca = \mu_o U / \gamma$ and Reynolds number $Re = \rho_o UH / \mu_c$ corresponding to this study are smaller than 0.01. Here, $\rho_o = 840 \text{ kg/m}^3$, $U = 0.75\text{--}8.5 \text{ mm/s}$ and $H = 75\text{--}200 \mu\text{m}$ are the density of the mineral oil, the total mean velocity and channel height, respectively.

In Fig. 4(d), we quantified the flow rate ratio of the branches by measuring the maximum fluid velocities in the bypass and the main channel using particle-tracking velocimetry. After trapping the drops using rectification, we pumped a solution of 0.5 wt. % hollow glass beads ($3 \mu\text{m}$ diameter, Polysciences, Inc.) in mineral oil into the MPN. The tracer particles were tracked at the intersection of the horizontal and vertical mid planes (along the height and the width of the channel) in both the main channel and the bypass of the loop. The measured velocity of these tracer particles at the midplane corresponds to the maximum fluid velocity (V_{max}) in the respective channel. The average fluid velocity and flow rate is then given by

$$V_{\text{avg}} = \beta V_{\text{max}}, \quad (2)$$

$$Q = V_{\text{avg}} A, \quad (3)$$

where β is proportionality constant that depends on the height and width of the channel and A is the cross sectional area of the channel. The proportionality constant β is the same for the main channel and the bypass as the height and width of these channels are identical. Therefore, the ratio of flow rates in the main channel and the bypass ($\frac{Q_M}{Q_B}$) can be found by

$$\frac{Q_M}{Q_B} = \frac{V_{\text{avg},M} A}{V_{\text{avg},B} A} = \frac{\beta V_{\text{max},M}}{\beta V_{\text{max},B}} = \frac{V_{\text{max},M}}{V_{\text{max},B}}. \quad (4)$$

In Eq. (4), the subscript index M and B refer to main channel and bypass, respectively.

Since $V_{\text{max},M}$ and $V_{\text{max},B}$ are measured experimentally, Eq. (4) allows us to determine the flow rate ratio between the trap and the bypass channel ($\frac{Q_T}{Q_B}$) as

$$\frac{Q_T}{Q_B} = \frac{Q_M}{Q_B} - 1. \quad (5)$$

D. Data analysis

All images and movies were analyzed using Image J v.1.43r. The volume of drops (V_d) in the train was calculated by measuring the length of the drop and then multiplying by the width and height of the channel. This method of calculating V_d yielded values that are within 2% of the values that would be obtained by taking the ratio of aqueous flow rate to droplet production frequency.

To quantify the polydispersity in the static drop array generated from either coalescing or non-coalescing drops, we measured the volume of trapped drops, and defined the polydispersity as percentage of the coefficient of variance of volume of trapped drops in the array. The volume of trapped drop (V_T) was calculated by multiplying the projected area of the droplet from the image with the height of the device. We verified that this approach was sufficiently accurate by comparing the volume of the drops before and after parking (by analyzing the movie where there was no drop fragmentation), and found them to differ by less than 1.5%. The static drop array was considered to be monodisperse when the polydispersity was between 1%–5%.

E. Simulation of drop traffic in MPN

The traffic model is based on treating drops as point objects that impose a fixed flow resistance.³¹ At a junction, drops always choose the branch with the highest flow rate. The flow rates

and pressure drop in branches are computed using relations analogous to Kirchhoff's laws for electrical circuits. Details of the simulation algorithm and the choice of modeling parameters are described in supplementary material text 1.3.³⁶

ACKNOWLEDGMENTS

This work was funded by an NSF CAREER Award (Grant No. 1160836) to S.A.V. Additionally, S.S.B. and W.S.W. were supported by NSF Grant (Nos. 967172 and 1124814). J.B. acknowledges financial support from NSF Grant No. 1059745.

- ¹P. S. Dittrich and A. Manz, "Lab-on-a-chip: microfluidics in drug discovery," *Nat. Rev. Drug Discovery* **5**, 210–218 (2006).
- ²R. Macarron *et al.*, "Impact of high-throughput screening in biomedical research," *Nat. Rev. Drug Discovery* **10**, 188–195 (2011).
- ³D. G. Anderson, S. Levenberg, and R. Langer, "Nanoliter-scale synthesis of arrayed biomaterials and application to human embryonic stem cells," *Nat. Biotechnol.* **22**, 863–866 (2004).
- ⁴M. Y. Lee *et al.*, "Three-dimensional cellular microarray for high-throughput toxicology assays," *Proc. Natl. Acad. Sci. U.S.A.* **105**, 59–63 (2008).
- ⁵P. C. Simpson *et al.*, "High-throughput genetic analysis using microfabricated 96-sample capillary array electrophoresis microplates," *Proc. Natl. Acad. Sci. U.S.A.* **95**, 2256–2261 (1998).
- ⁶E. A. Ottesen, J. W. Hong, S. R. Quake, and J. R. Leadbetter, "Microfluidic digital PCR enables multigene analysis of individual environmental bacteria," *Science* **314**, 1464–1467 (2006).
- ⁷C. Hansen and S. R. Quake, "Microfluidics in structural biology: smaller, faster, better," *Curr. Opin. Struct. Biol.* **13**, 538–544 (2003).
- ⁸L. Li *et al.*, "Nanoliter microfluidic hybrid method for simultaneous screening and optimization validated with crystallization of membrane proteins," *Proc. Natl. Acad. Sci. U.S.A.* **103**, 19243–19248 (2006).
- ⁹D. A. Dunn and I. Feygin, "Challenges and solutions to ultra-high-throughput screening assay miniaturization: submicroliter fluid handling," *Drug Discovery Today* **5**, S84–S91 (2000).
- ¹⁰T. V. Murthy, D. Kroncke, and P. D. Bonin, "Adding precise nanoliter volume capabilities to liquid-handling automation for compound screening experimentation," *J. Lab Autom.* **16**, 221–228 (2011).
- ¹¹H. Song, D. L. Chen, and R. F. Ismagilov, "Reactions in droplets in microfluidic channels," *Angew. Chem. Int. Ed.* **45**, 7336–7356 (2006).
- ¹²S. Y. Teh, R. Lin, L. H. Hung, and A. P. Lee, "Droplet microfluidics," *Lab Chip* **8**, 198–220 (2008).
- ¹³D. T. Chiu, R. M. Lorenz, and G. D. M. Jeffries, "Droplets for ultrasmall-volume analysis," *Anal. Chem.* **81**, 5111–5118 (2009).
- ¹⁴M. T. Guo, A. Rotem, J. A. Heyman, and D. A. Weitz, "Droplet microfluidics for high-throughput biological assays," *Lab Chip* **12**, 2146–2155 (2012).
- ¹⁵G. F. Christopher and S. L. Anna, "Microfluidic methods for generating continuous droplet streams," *J. Phys. D: Appl. Phys.* **40**, R319–R336 (2007).
- ¹⁶R. Dangla, S. C. Kayi, and C. N. Baroud, "Droplet microfluidics driven by gradients of confinement," *Proc. Natl. Acad. Sci. U.S.A.* **110**, 853–858 (2013).
- ¹⁷E. Brouzes *et al.*, "Droplet microfluidic technology for single-cell high-throughput screening," *Proc. Natl. Acad. Sci. U.S.A.* **106**, 14195–14200 (2009).
- ¹⁸O. J. Miller *et al.*, "High-resolution dose-response screening using droplet-based microfluidics," *Proc. Natl. Acad. Sci. U.S.A.* **109**, 378–383 (2012).
- ¹⁹J. J. Agresti *et al.*, "Ultrahigh-throughput screening in drop-based microfluidics for directed evolution," *Proc. Natl. Acad. Sci. U.S.A.* **107**, 4004 (2010).
- ²⁰A. C. Hatch *et al.*, "1-Million droplet array with wide-field fluorescence imaging for digital PCR," *Lab Chip* **11**, 3838–3845 (2011).
- ²¹R. R. Pompano, W. S. Liu, W. B. Du, and R. F. Ismagilov, "Microfluidics using spatially defined arrays of droplets in one, two, and three dimensions," *Annu. Rev. Anal. Chem.* **4**, 59–81 (2011).
- ²²W. W. Shi, J. H. Qin, N. N. Ye, and B. C. Lin, "Droplet-based microfluidic system for individual caenorhabditis elegans assay," *Lab Chip* **8**, 1432–1435 (2008).
- ²³A. Huebner *et al.*, "Static microdroplet arrays: a microfluidic device for droplet trapping, incubation and release for enzymatic and cell-based assays," *Lab Chip* **9**, 692–698 (2009).
- ²⁴H. Boukellal, S. Selimovic, Y. W. Jia, G. Cristobal, and S. Fraden, "Simple, robust storage of drops and fluids in a microfluidic device," *Lab Chip* **9**, 331–338 (2009).
- ²⁵W. B. Du, L. Li, K. P. Nichols, and R. F. Ismagilov, "SlipChip," *Lab Chip* **9**, 2286–2292 (2009).
- ²⁶C. H. J. Schmitz, A. C. Rowat, S. Koster, and D. A. Weitz, "Dropspots: a picoliter array in a microfluidic device," *Lab Chip* **9**, 44–49 (2009).
- ²⁷D. E. Cohen, T. Schneider, M. Wang, and D. T. Chiu, "Self-digitization of sample volumes," *Anal. Chem.* **82**, 5707–5717 (2010).
- ²⁸P. Abbyad, R. Dangla, A. Alexandrou, and C. N. Baroud, "Rails and anchors: guiding and trapping droplet microreactors in two dimensions," *Lab Chip* **11**, 813–821 (2011).
- ²⁹M. Sun, S. S. Bithi, and S. A. Vanapalli, "Microfluidic static droplet arrays with tuneable gradients in material composition," *Lab Chip* **11**, 3949–3952 (2011).
- ³⁰S. S. Bithi and S. A. Vanapalli, "Behavior of a train of droplets in a fluidic network with hydrodynamic traps," *Biomicrofluidics* **4**, 044110–044119 (2010).

- ³¹M. Schindler and A. Ajdari, "Droplet traffic in microfluidic networks: A simple model for understanding and designing," *Phys. Rev. Lett.* **100**, 044501 (2008).
- ³²G. K. Kurup and A. S. Basu, "Field-free particle focusing in microfluidic plugs," *Biomicrofluidics* **6**, 022008–022017 (2012).
- ³³M. Sun, Z. S. Khan, and S. A. Vanapalli, "Blood plasma separation in a long two-phase plug flowing through disposable tubing," *Lab Chip* **12**, 5225–5230 (2012).
- ³⁴L. Menetrier-Deremble and P. Tabeling, "Droplet breakup in microfluidic junctions of arbitrary angles," *Phys. Rev. E* **74**, 035303 (2006).
- ³⁵H. Bruus, *Theoretical Microfluidics* (OUP, Oxford, 2008).
- ³⁶See supplementary material at <http://dx.doi.org/10.1063/1.4885079> for the calculation of throughput of drop storage and parking, device dimensions and flow conditions used in this study and simulation of drop traffic in microfluidic parking networks.
- ³⁷T. Thorsen, S. J. Maerkl, and S. R. Quake, "Microfluidic large-scale integration," *Science* **298**, 580–584 (2002).
- ³⁸C. Priest, S. Herminghaus, and R. Seemann, "Controlled electrocoalescence in microfluidics: Targeting a single lamella," *Appl. Phys. Lett.* **89**, 134101–134103 (2006).
- ³⁹A. R. Abate, T. Hung, P. Mary, J. J. Agresti, and D. A. Weitz, "High-throughput injection with microfluidics using picoinjectors," *Proc. Natl. Acad. Sci. U.S.A.* **107**, 19163–19166 (2010).
- ⁴⁰D. C. Duffy, J. C. McDonald, O. J. Schueller, and G. M. Whitesides, "Rapid prototyping of microfluidic systems in poly(dimethylsiloxane)," *Anal. Chem.* **70**, 4974–4984 (1998).
- ⁴¹F. Malloggi, H. Gu, A. G. Banpurkar, S. A. Vanapalli, and F. Mugele, "Electrowetting - A versatile tool for controlling microdrop generation," *Eur. Phys. J. E* **26**, 91–96 (2008).
- ⁴²L. Mazutis and A. D. Griffiths, "Selective droplet coalescence using microfluidic systems," *Lab Chip* **12**, 1800–1806 (2012).